Blind SAR ADC Capacitor Mismatch Calibration

Armia Salib, Mark F. Flanagan and Barry Cardiff

School of Electrical and Electronic Engineering, University College Dublin, Ireland

Email: armia.salib-farag@ucdconnect.ie, mark.flanagan@ieee.org, barry.cardiff@ucd.ie

***Abstract*—This paper presents an all-digital background blind calibration technique for the capacitor mismatch problem in SAR ADCs. It utilizes the redundancy offered using a sub-radix-2 DAC architecture to blindly estimate the mismatch and the assigned weight for each comparator decision. The weights are estimated by building *partial* histogram windows for the comparator decision vectors. To remove the dependency on the input signal's probability density function, the histogram windows are normalized with respect to their peaks. Matlab simulation results show that an ENOB within 0.12bit of the optimal is attained using the proposed algorithm.**

***Index terms*—SAR ADC, capacitor mismatch, calibration.**

I. INTRODUCTION

Due to variations in the fabrication process, the values of the fabricated capacitors in a typical SAR ADC differ from their nominal values. Prior to the advent of digital calibration techniques, the output of such a SAR ADC had only moderate resolution, and it was necessary to choose the capacitor sizes to be sufficiently large so as to reduce the effect of mismatch [4]. However, by including capacitor mismatch calibration, this is no longer the case, and the capacitor sizes are now designed according to thermal noise considerations only, leading to faster ADCs having lower power and a smaller silicon area [4].

There are two main types of calibration techniques: foreground and background. In the foreground techniques, an offline calibration process is used to compute calibration weights that are then applied during normal operation. For example, in [3] calibration weights are iteratively updated to make uniform the ADC's output histogram for a uniformly distributed input injected prior to normal operation. Foreground calibration works well when the overall system is such that a calibration startup phase can be allocated, and where the adaptation of the weights during normal operation is not required.

In the background techniques, the calibration weights are computed during normal operation and updated continuously. This is useful in applications where no startup phase is allocated, and where the calibration weights need to be adjusted over time. For example, in [2], a histogram is measured covering *all* possible comparator decision vectors, and the weights are extracted by solving an *overdetermined* system of linear equations to average the effect of the input distribution.

The techniques presented in [1-3] utilize redundancy through a sub-radix-2 architecture to avoid the occurrence of the super-radix-2 condition [1]. This condition occurs when one capacitor is larger than the sum of all smaller capacitors, and causes at least one output vector to appear for a wide input voltage range. The use of sub-radix-2 enables obtaining a histogram of comparator decision vectors with rich evenly distributed equal-level peaks for a uniformly distributed input signal, even if mismatch exists.

This publication has emanated from research supported by S3group, Dublin, Ireland, and in part by a research grant from Science Foundation Ireland (SFI) and is co-funded under the European Regional Development Fund under Grant Number 13/RC/2077.

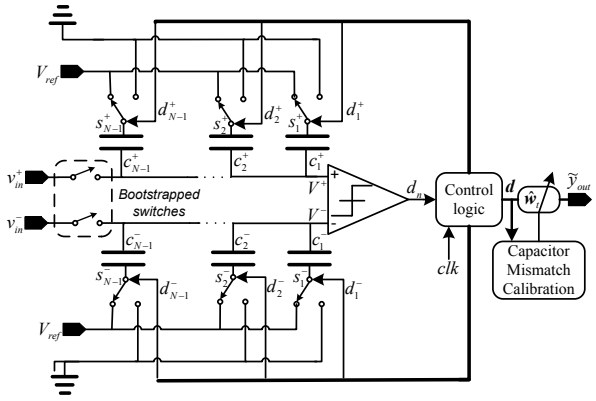

Fig. 1. Block diagram for a SAR ADC (from [5]).

In this paper, we further exploit the sub-radix-2 architecture properties to enable *blind* calibration independent of the input signal's probability density function (PDF), meaning that there is no requirement to alter the analog frontend circuit. The calibration weights are estimated by constructing exactly N equations. These are obtained by building the histogram for the comparator vector output at certain ranges. This reduces the histogram memory size to only 5.8% compared to other approaches that require sensing the full histogram. The proposed algorithm attains an effective number of bits (ENOB) within 0.12bit of the optimal, even in the existence of imperfections.

II. SAR ADC MODEL

In SAR ADCs, a complete conversion can be divided into three phases; 1) Acquisition: the analog input signal is sampled into the capacitor banks. 2) Searching: N successive decisions are made by a comparator, during which controlled switches are configured to minimize the voltage across the comparator's inputs. 3) Post processing: the N comparator decisions are processed to deliver B bits at the ADC's output.

Fig. 1 shows the block diagram for a SAR ADC based on the monotonic capacitor switching architecture reported in [5]; note however that our proposed calibration algorithm and analysis are also valid for other architectures. Two banks of capacitors, $\boldsymbol{c}^+$ and $\boldsymbol{c}^-$, are connected to the terminals V^+ and V^- of the comparator, respectively. Each bank consists of $N-1$ sub-radix-2 weighted capacitors with nominal values $c_i^+ = c_i^- = \mathfrak{r}^{i-1} c_u \ \forall i \in \{1, .. N-1\}$, where c_u is a unit capacitance and $\mathfrak{r} < 2$ is the chosen radix [1]. Both $\boldsymbol{c}^+$ and $\boldsymbol{c}^-$ are connected to switches controlled by the binary vectors $\boldsymbol{d}^+$ and $\boldsymbol{d}^-$, respectively. Each switch connects a capacitor to the reference voltage V_{ref} when the corresponding control bit is 1, and to ground otherwise. For any $\boldsymbol{d}^+$ and $\boldsymbol{d}^-$, the voltage on V^+ and V^- can be expressed by (1) where $\overline{x}$ denotes the complement of a bit x.

$$V^{(+/-)} = v_{in}^{(+/-)} - \frac{V_{ref}}{\sum c_l^{(+/-)}} \sum_{i=1}^{N-1} \overline{d_i^{(+/-)}} c_i^{(+/-)}. \qquad (1)$$

During the acquisition phase, the control bits in $\boldsymbol{d}^+$ and $\boldsymbol{d}^-$ are all initialized to 1, and the input voltage v_{in} is applied differentially across v_{in}^+ and v_{in}^- which in turn are connected to V^+ and V^- respectively via the bootstrapped switches.

The searching phase consists of N steps indexed from $n = N-1$ down to 0. In each step n, a comparator decision is made on d_n according to

$$d_n = \begin{cases} 1, & \text{when } e_n(v_{in}) > 0 \\ 0, & \text{otherwise,} \end{cases} \tag{2}$$

where $e_n(v_{in}) \triangleq V_n^+ - V_n^-$ is the residual voltage on the n^{th} step for a given v_{in}. From (1), this can be expressed as

$$e_n(v_{in}) = v_{in} - \frac{V_{ref}}{\sum c_l^+} \sum_{i=n+1}^{N-1} (d_i(c_i^+ + \dot{c}_i^-) - \dot{c}_i^-), \tag{3}$$

$$\dot{c}_i^- = c_i^- \frac{\sum c_l^+}{\sum c_l^-}, \forall i \in \{1, .., N-1\}. \tag{4}$$

To minimize the residual voltage in the next step, $e_{n+1}(v_{in})$, the control bits of the switches are accordingly configured to $d_n^+ = \overline{d_n}$ and $d_n^- = d_n$ on all but the last step.

To find bounds on v_{in} after resolving each d_n, consider the smallest $k > n$ for which $d_k = \overline{d_n}$ (i.e., $d_i = d_n \; \forall i \in \{n, n+1, \ldots, k-1\}$). Consider first the case $d_n = 0$. Here we have $e_k(v_{in}) > 0$ and $e_n(v_{in}) < 0$; thus we can use (3) to derive bounds on v_{in} in terms of the resolved decisions:

$$\begin{aligned} \frac{V_{ref}}{\sum c_l^+} \sum_{i=k+1}^{N-1} (d_i(c_i^+ + \dot{c}_i^-) - \dot{c}_i^-) < v_{in} \\ < \frac{V_{ref}}{\sum c_l^+} \sum_{i=n+1}^{N-1} (d_i(c_i^+ + \dot{c}_i^-) - \dot{c}_i^-), \end{aligned} \tag{5}$$

and therefore v_{in} can be written as a fixed quantity and a random variable (RV) term, i.e.,

$$v_{in} = \frac{V_{ref}}{\sum c_l^+} \left(\delta_{n,k} + \sum_{i=n+1}^{N-1} (d_i(c_i^+ + \dot{c}_i^-) - \dot{c}_i^-) \right), \tag{6}$$

where $\delta_{n,k}$ is a RV on the range $\left[-(c_k^+ - \sum_{i=n+1}^{k-1} \dot{c}_i^-), 0\right]$. Here $\delta_{n,k}$ appears due to the quantization error; i.e., the breadth of its range is minimum when n=0. In this case, it can be shown that $\delta_{0,k} \in [-c_1^+, 0] \;\; \forall k > 0$ (this can be obtained by letting $k = 1$). Similarly, it can be shown that (6) also holds for the case $d_n = 1$, where $\delta_{n,k} \in \left[0, \dot{c}_k^- - \sum_{i=n+1}^{k-1} c_i^+\right]$. Combining the results in both cases when $n = 0$ and $k = 1$ yields

$$v_{in} = \frac{V_{ref}}{\sum c_l^+} \left(\sum_{i=1}^{N-1} (d_i(c_i^+ + \dot{c}_i^-) - \dot{c}_i^-) + \frac{d_0(c_1^+ + \dot{c}_1^-) - \dot{c}_1^-}{2} + n_q \right), \tag{7}$$

i.e., v_{in} can be expressed as the sum of a linear combination of $\{d_i\}$, a fixed offset, and a quantization noise n_q, where $n_q \in [-c_1^+/2, c_1^+/2]$ when d_n=0, and $n_q \in [-\dot{c}_1^-/2, \dot{c}_1^-/2]$ otherwise.

A weighted sum of the decisions can be computed as

$$y_{out} = \sum_{i=0}^{N-1} w_i \, d_i = \boldsymbol{w}^{\mathrm{T}} \, \boldsymbol{d}, \tag{8}$$

where $\boldsymbol{d} = \{d_i\}$ and $\boldsymbol{w} = \{w_i\}$ are $N \times 1$ vectors of comparator decisions and weights, respectively. Ignoring the offset term in (7), and selecting these weights to be

$$w_i \propto (c_i^+ + \dot{c}_i^-), \forall i \in \{1, .. N-1\}, \tag{9}$$

$$w_0 = w_1/2, \tag{10}$$

maximizes the ENOB; such weights are *optimal* in this sense.

Knowledge of the values of the fabricated capacitances permits the computation of $\boldsymbol{w}$, and hence of the value of y_{out}. However, in real applications the exact values of the fabricated capacitances are not known, leading to ADC performance degradation, and thus raising the need for calibration.

III. Comparator Noise and Settling Time

For a realistic SAR ADC model, the following sources of imperfection, which directly affect the capacitor mismatch estimation, are considered in verifying the proposed technique.

In practice, a finite time period τ_s is allocated after each switch change for the settling of the DAC's voltage, which is needed to settle within ½ LSB for radix-2 DACs. However, in sub-radix-2 DACs, τ_s can be shortened, permitting settling errors that can be corrected in later steps [6]. To model the settling error, the DAC is considered as a first-order system with time constant τ, and (3) can be modified to

$$e_n(v_{in}) = v_{in} - \frac{V_{ref}}{\sum c_l^+} \sum_{i=n+1}^{N-1} (d_i(c_i^+ + \dot{c}_i^-) - \dot{c}_i^-)(1 - e^{\frac{-(i-n)\tau_s}{\tau}}). \tag{11}$$

Also, SAR ADCs suffer from different noise sources where the comparator noise power dominates by a factor of 100 over the others [6]. To model the comparator noise, (2) is modified to

$$d_n = \begin{cases} 1, & \text{for } e_n(v_{in}) + \eta_n > 0 \\ 0, & \text{otherwise,} \end{cases} \tag{12}$$

where η_n is a Gaussian-distributed RV with input-referred standard deviation σ_c.

IV. Calibration Scheme

The goal of the proposed calibration algorithm is to estimate $\boldsymbol{w}$; this can be achieved by creating exactly N equations relating the unknown $\boldsymbol{w}$ to the probability mass function (PMF) of $\boldsymbol{d}$.

First, we need to define two mappings. The mapping $\emptyset(\boldsymbol{d})$ maps $\boldsymbol{d}$ to the lowest input voltage generating $\boldsymbol{d}$, which, with reference to (7), can be expressed as

$$\emptyset(\boldsymbol{d}) \triangleq \alpha \sum_{i=0}^{N-1} w_i d_i + \beta \quad , \tag{13}$$

where α and β are constants dictated by (7). Also, $\theta(\boldsymbol{d})$ maps $\boldsymbol{d}$ to a unique integer value via

$$\theta(\boldsymbol{d}) \triangleq \sum_{i=0}^{N-1} 2^i d_i. \tag{14}$$

A. Probability mass function characteristic of the SAR ADC

Let $\boldsymbol{h} = \{h_i\}$ denote the PMF over all 2^N possible values of the decision vector $\boldsymbol{d}$; this depends on the PDF of v_{in}, which we denote by $f(v_{in})$. Fig. 2 shows an example of a measured $\boldsymbol{h}$ for the case of r=1.8, N=8 and a uniformly distributed input signal.

Note that there exist some vectors $\boldsymbol{d}$ which *cannot* be observed at the ADC output; we call such vectors *inactive* (all other vectors are *active*). This behavior can be seen from Fig. 2. To illustrate why this occurs, consider a vector $\boldsymbol{d}$ with $d_n = 0$ for some n, and consider the smallest $k > n$ for which $d_k = \overline{d_n}$. Whenever it happens that $c_k^+ < \sum_{i=n+1}^{k-1} \dot{c}_i^-$, then the lower bound in (5) exceeds the upper bound, and it follows that any such vector $\boldsymbol{d}$ is inactive (as there is no valid solution for v_{in}). A similar reasoning applies for the case $d_n = 1$. Extending this argument, it can be shown that for nominal capacitance values and ignoring settling errors, the vector $\boldsymbol{d}$ is inactive whenever

$$k - n > \frac{\log(2\mathrm{r}^{-1} - 1)}{\log(\mathrm{r}^{-1})} \triangleq \epsilon, \tag{15}$$

i.e., active vectors are not expected to have $\lceil \epsilon \rceil$ successive equal comparator decisions. This result gives rise to many inactive vectors forming contiguous *gaps* as can be observed in Fig. 2.

B. Input-output statistical relationship of the SAR ADC

Due to the searching mechanism used in sub-radix-2 SAR ADCs, the relationship between $\emptyset(.)$ and $\theta(.)$ is monotonic; for any pair of active vectors $\boldsymbol{\ell}$ and $\boldsymbol{r}$, $\theta(\boldsymbol{\ell}) < \theta(\boldsymbol{r})$ is guaranteed when $\emptyset(\boldsymbol{\ell}) < \emptyset(\boldsymbol{r})$. Using this property, we can conclude that $P(\theta(\boldsymbol{\ell}) \le \theta(\boldsymbol{d}) < \theta(\boldsymbol{r})) = P(\emptyset(\boldsymbol{\ell}) \le v_{in} < \emptyset(\boldsymbol{r}))$, where $P(x)$ denotes the probability of an event x. Hence, we can express the relationship between $\boldsymbol{h}$ and $f(v_{in})$ by

$$\begin{aligned}\sum_{i=\theta(\boldsymbol{\ell})}^{\theta(\boldsymbol{r})-1} h_i &= P\big(\emptyset(\boldsymbol{\ell}) \le v_{in} < \emptyset(\boldsymbol{r})\big) \\ &= \int_{\emptyset(\boldsymbol{\ell})}^{\emptyset(\boldsymbol{r})} f(v_{in})\, dv_{in} \\ &= \rho(\boldsymbol{\ell},\boldsymbol{r})(\emptyset(\boldsymbol{r}) - \emptyset(\boldsymbol{\ell})) \\ &= \alpha\rho(\boldsymbol{\ell},\boldsymbol{r}) \sum_{i=0}^{N-1} w_i\, (r_i - \ell_i),\end{aligned} \tag{16}$$

where $\rho(\boldsymbol{\ell},\boldsymbol{r})$ is the average of $f(v_{in})$ over the range $[\emptyset(\boldsymbol{\ell}), \emptyset(\boldsymbol{r})]$.

C. Constructing a system of equations

Using (16), N equations (indexed by $k \in \{0,..N-1\}$) are constructed to find $\boldsymbol{w}$. For the k^{th} equation, two *nearly consecutive* active vectors, $\boldsymbol{\ell}^{(k)}$ and $\boldsymbol{r}^{(k)}$, are selected such that $\ell_k^{(k)} = 0$, $r_k^{(k)} = 1$ and $\ell_i^{(k)} = r_i^{(k)}\ \forall i > k$. Then (16) can be written as

$$\sum_{i=\theta(\boldsymbol{\ell}^{(k)})}^{\theta(\boldsymbol{r}^{(k)})-1} h_i = \alpha\rho_k \sum_{i=0}^{k} w_i \left(r_i^{(k)} - \ell_i^{(k)}\right), \tag{17}$$

where $\rho_k \triangleq \rho\left(\boldsymbol{\ell}^{(k)}, \boldsymbol{r}^{(k)}\right)$. In matrix form, we may write

$$w_0\, \boldsymbol{p}^{\mathrm{T}} = \boldsymbol{w}^{\mathrm{T}}\, (\boldsymbol{\mathcal{R}} - \boldsymbol{\mathcal{L}}) = \boldsymbol{w}^{\mathrm{T}}\, \boldsymbol{U}, \tag{18}$$

where $\boldsymbol{\mathcal{L}}$ (resp. $\boldsymbol{\mathcal{R}}$) is an $N \times N$ matrix whose k^{th} column is $\boldsymbol{\ell}^{(k)}$ (resp. $\boldsymbol{r}^{(k)}$), $\boldsymbol{U} \triangleq \boldsymbol{\mathcal{R}} - \boldsymbol{\mathcal{L}}$ is an upper triangular matrix with all entries on the main diagonal equal to 1, and the k^{th} element in the $N \times 1$ vector $\boldsymbol{p}$ can be written as

$$p_k = \sum_{i=\theta(\boldsymbol{\ell}^{(k)})}^{\theta(\boldsymbol{r}^{(k)})-1} \frac{h_i}{\alpha\rho_k w_0}. \tag{19}$$

Ignoring the ADC's gain, we can map the maximum y_{out} computed in (8) to match the maximum quantized B-bit output:

$$\sum_{i=0}^{N-1} w_i = 2^B - 1. \tag{20}$$

Using (18) and (20), $\boldsymbol{w}$ can be evaluated according to

$$\boldsymbol{w}^{\mathrm{T}} = \frac{2^B - 1}{\|\boldsymbol{p}^{\mathrm{T}}\boldsymbol{U}^{-1}\|_1} \boldsymbol{p}^{\mathrm{T}}\boldsymbol{U}^{-1}. \tag{21}$$

In the example shown in Fig. 2, a gap generated by a change in d_7 is depicted. The vectors lying on the left of this gap have $d_7 = 0$, and the vectors on the right have $d_7 = 1$. To construct the 7^{th} equation, we need to select an active vector $\boldsymbol{\ell}^{(7)}$ from the left of this gap, and similarly a vector $\boldsymbol{r}^{(7)}$ from its right.

D. Determining the peak level

From Fig. 2, we can notice that $\boldsymbol{h}$ richly contains peaks that are almost evenly distributed, and have equal level for uniform $f(v_{in})$ (this is due to the assumption that the super-radix-2 condition does not occur). We are interested in finding their

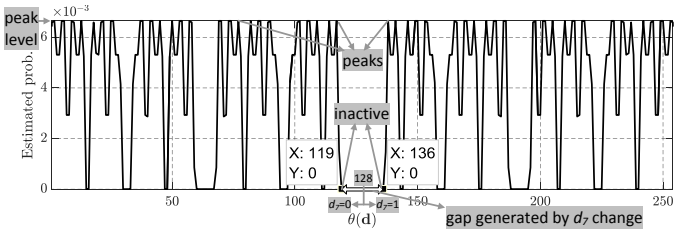

Fig. 2. A measurement of $\boldsymbol{h}$ with $\mathfrak{r}$=1.8 and N=8, for a uniformly distributed input signal.

level, λ_k, around the selected vectors for the k^{th} equation. Which depends directly on two factors:

1) The input signal's PDF, $f(v_{in})$, that is assumed to be locally uniform in this region and equals ρ_k. We can notice its effect in Fig. 3 where $\boldsymbol{h}$ is modulated by $f(v_{in})$.

2) The maximum voltage breadth at which a certain vector $\boldsymbol{d}$ appears, it is directly proportional to the maximum breadth for $\delta_{0,k}$, which in turn is proportional to w_0.

Hence, we can write λ_k in the form (22), where γ is a constant of proportionality. This can be used to replace $\rho_k w_0$ in (19). Note however that in practice, both constants α and γ can be ignored due to the normalization in (21).

$$\lambda_k = \gamma\rho_k w_0. \tag{22}$$

V. Calibration Implementation

The previous section described the mathematical framework for the proposed algorithm. In this section we illustrate the methods used to construct these equations.

In the following discussion, a tilde above any mathematical symbol denotes an *estimate* of the corresponding variable. An exception to this rule is $\tilde{\boldsymbol{h}}$, which denotes the comparator decision vector histogram - this is measured by monitoring M decision vectors, and its i^{th} element $\tilde{h}_i$ contains the *number* of observed events where $\theta(\boldsymbol{d}) = i$.

Although we have N unknowns in $\boldsymbol{w}$, there are only $N-2$ degrees of freedom due to the constraints imposed by (10) and (20); therefore we set p_0=1, and the equation indexed by k=1 is selected to satisfy (10) via setting $r_0^{(1)}$=0, $\ell_0^{(1)}$=1 and p_1=1.

In the proposed calibration technique, a calibration cycle is divided into three phases. Each phase requires observing a chunk of M comparator decision vectors. Let $\boldsymbol{d}(m)$ denote the m^{th} decision vector in the considered chunk.

Due to the existence of imperfections, many inactive vectors can appear with low probability, making direct identification of $\widetilde{\boldsymbol{\mathcal{L}}}$ and $\widetilde{\boldsymbol{\mathcal{R}}}$ impractical. Instead, we first identify $\dot{\boldsymbol{\mathcal{L}}}$ and $\ddot{\boldsymbol{\mathcal{R}}}$, which are *coarse* estimates of $\widetilde{\boldsymbol{\mathcal{L}}}$ and $\widetilde{\boldsymbol{\mathcal{R}}}$. In the following discussion, $\dot{\boldsymbol{\mathcal{L}}}$ is identified in the first phase, and $\ddot{\boldsymbol{\mathcal{R}}}$ in the second; however, this ordering can freely be swapped. Subsequently, in the third phase, *partial histogram windows* are built around the vectors in $\dot{\boldsymbol{\mathcal{L}}}$ and $\ddot{\boldsymbol{\mathcal{R}}}$, and these are used to accurately identify $\widetilde{\boldsymbol{\mathcal{L}}}$, $\widetilde{\boldsymbol{\mathcal{R}}}$ and $\tilde{\boldsymbol{p}}$.

In the first phase, the k^{th} column in $\dot{\boldsymbol{\mathcal{L}}}$, $\dot{\boldsymbol{\ell}}^{(k)}$, is identified $\forall k \in \{2,..,N-1\}$. We select $\ddot{\boldsymbol{\ell}}^{(k)}$ to be the first decision vector located on the histogram just on the left of a gap created by a change in the decision d_k, which can be found using a running maximum over M outputs

$$\ddot{\boldsymbol{\ell}}^{(k)} = \underset{\boldsymbol{d}(m)}{\operatorname{argmax}} \sum_{i=0}^{k} 2^i d_i(m)\,, \text{subject to } d_k(m) = 0. \tag{23}$$

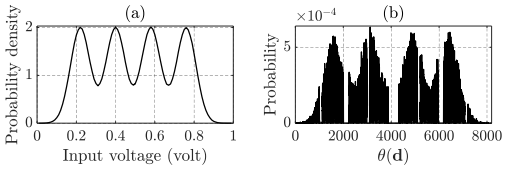

Fig. 3. (a) Input signal PDF, $f(v_{in})$; (b) $\boldsymbol{h}$.

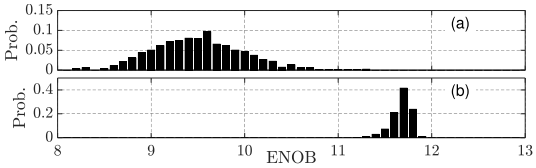

Fig. 4. ENOB distribution (a) without calibration; (b) with calibration. Here $\tau_s = 3\tau$ and $\sigma_c = 0\mu V$.

To make sure that the chosen $\ddot{\boldsymbol{\ell}}^{(k)}$ is on a gap created by a change in the decision d_k, we make use of the result obtained in (15): vectors $\boldsymbol{d}(m)$ with $\lfloor \epsilon - 0.5 \rfloor$ or more consecutive equal decisions within indices $\geq k$ are not considered in (23).

The second phase starts after identifying $\ddot{\boldsymbol{\mathcal{L}}}$, and another M vectors are used to identify $\ddot{\boldsymbol{\mathcal{R}}}$. The k^{th} column in $\ddot{\boldsymbol{\mathcal{R}}}$, $\ddot{\boldsymbol{r}}^{(k)}$, is the first decision vector located on the histogram just on the right of a gap created by a change in the decision d_k, which can be found using a running minimum over M outputs

$$\ddot{\boldsymbol{r}}^{(k)} = \underset{\boldsymbol{d}(m)}{\operatorname{argmin}} \sum_{i=0}^{k} 2^i d_i(m), \text{subject to } d_k(m) = 1 \text{ and } d_i(m) = \ddot{\ell}_i^{(k)} \; \forall i > k. \tag{24}$$

In the third phase, partial histogram windows are built on the two sides of each $\ddot{\boldsymbol{\ell}}^{(k)}$ and $\ddot{\boldsymbol{r}}^{(k)}$ pair, i.e., in the ranges $\theta(\boldsymbol{d}) \in \left[\theta\left(\ddot{\boldsymbol{\ell}}^{(k)}\right) - \gamma_k, \theta\left(\ddot{\boldsymbol{\ell}}^{(k)}\right)\right]$ and $\theta(\boldsymbol{d}) \in \left[\theta\left(\ddot{\boldsymbol{r}}^{(k)}\right), \theta\left(\ddot{\boldsymbol{r}}^{(k)}\right) + \gamma_k\right]$, where γ_k is a selected positive integer. For each partial histogram, the estimate $\tilde{\lambda}_k$ of the peak level is calculated by evaluating the median of the peaks in the k^{th} window.

A threshold proportional to $\tilde{\lambda}_k$ is used to exclude inactive vectors which appear due to noise. Accordingly, both $\tilde{\boldsymbol{\ell}}^{(k)}$ and $\tilde{\boldsymbol{r}}^{(k)}$ are chosen, and $\tilde{p}_k$ is evaluated according to (19) and (22).

After identifying $\tilde{\boldsymbol{\mathcal{L}}}$, $\tilde{\boldsymbol{\mathcal{R}}}$ and $\tilde{\boldsymbol{p}}$, (21) can be used to estimate the weights in calibration cycle t, $\tilde{\boldsymbol{w}}_t$. And accordingly $\hat{\boldsymbol{w}}_t$ is calculated as a weighted sum of the current and previous estimate, using a weighting factor μ, via

$$\hat{\boldsymbol{w}}_t = (1-\mu)\hat{\boldsymbol{w}}_{t-1} + \mu\tilde{\boldsymbol{w}}_t. \tag{25}$$

This is then used in (8) to produce the calibrated sample.

VI. Results

Matlab simulations are used to verify the proposed algorithm targeting a SAR ADC with $\mathfrak{r} = 1.86$, $N = 13$ and $B = 11$. The algorithm is configured to $M = 2^{18}$, the total number of memory words required to measure the histogram windows is 478, and each word is 8 bits. Two Monte Carlo simulations are used to verify the proposed technique. In both tests $\tau_s = 3\tau$, and 1000 capacitance sets are used where the unit capacitances suffer from mismatch having Gaussian distribution with standard deviation $\sigma_u = 0.08c_u$. A 4-level pulse amplitude modulation (4-PAM) input signal is used; the PDF $f(v_{in})$ and $\boldsymbol{h}$ are shown in Fig. 3. All reported results here are obtained after 16 calibration cycles.

In the first test, $\sigma_c = 0\mu V$ and hence the performance is limited mainly by the uncalibrated capacitor mismatch and the quantization noise. Fig. 4 shows the ENOB distributions obtained with and without calibration. Using optimal weights, the average ENOB is 11.9 bits. With calibration, the average ENOB is improved from 9.5 to 11.7 bits.

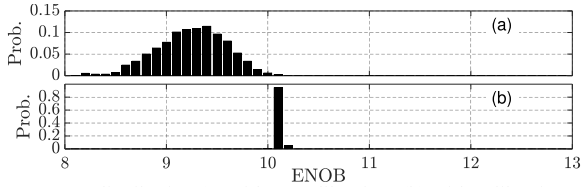

Fig. 5. ENOB distribution (a) without calibration; (b) with calibration. Here $\tau_s = 3\tau$ and $\sigma_c = 300\mu V$.

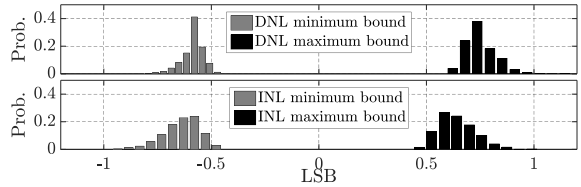

Fig. 6. Distributions of the INL and DNL bounds after calibration.

In the second test, Gaussian-distributed comparator noise with $\sigma_c = 300\mu V$ is applied. Similar to Fig. 4, Fig. 5 shows the results obtained for this test. The simulation shows that, using optimal weights, the average ENOB is 10.13 bits. With calibration, the average ENOB is improved from 9.24 to 10.12 bits. The maximum observed difference between the optimal and improved ENOB is 0.12 bits. The distributions of the INL and DNL bounds after calibration are shown in Fig. 6.

VII. Conclusion

A blind calibration technique has been presented for use with SAR ADCs. The technique senses the histogram bins only at the ranges we are interested in, to construct only N equations that are sufficient to estimate the weights, leading to a reduction in the required memory and making the proposed technique feasible. In the example tested, histogram bins were measured for only $478/2^{13}$=5.8% of all possible vectors. The proposed algorithm does not require any statistical constraints on the input signal except that this signal covers at least half of the ADC's input dynamic range. The presented results show that the ENOB is attained within 0.12bit of the optimal using this algorithm.

References

[1] W. Liu, P. Huang and Y. Chiu, "A 12-bit, 45-MS/s, 3-mW redundant successive-approximation-register analog-to-digital converter with digital calibration," *IEEE Journal of Solid-State Circuits*, vol. 46, no. 11, pp. 2661–2672, Aug. 2011.

[2] A. Chang, H. Lee and D. Boning, "A 12b 50MS/s 2.1mW SAR ADC with redundancy and digital background calibration," *IEEE ESSCIRC*, pp. 109–112, Sept. 2013.

[3] E. Swindlehurst and S. Chiang, "Histogram-based calibration of capacitor mismatch in SAR ADCs," *Electronics Letters*, vol. 51, no. 25, pp. 2096–2098, Dec. 2015.

[4] M. Ding, P. Harpe, Y. Liu, B. Busze, K. Philips and H. Groot, "A 46 µW 13 b 6.4 MS/s SAR ADC with background mismatch and offset calibration," *IEEE Journal of Solid-State Circuits*, vol. 52, no. 2, pp. 423–432, Feb. 2017.

[5] C. Liu, S. Chang, G. Huang and Y. Lin, "A 10-bit 50-MS/s SAR ADC with a monotonic capacitor switching procedure," *IEEE Journal of Solid-State Circuits*, vol. 45, no. 4, pp. 731–740, Mar. 2010.

[6] W. Paul Zhang and X. Tong, "Noise modeling and analysis of SAR ADCs," *IEEE Transactions on Very Large Scale Integration Systems*, vol. 23, no. 12, pp. 2922–2930, Dec. 2015.